Ultrathin 2D Photodetectors Utilizing Chemical Vapor Deposition Grown WS_2 with Graphene Electrodes

*Haijie Tan,[1] Ye Fan,[1] Yingqiu Zhou, [1] Qu Chen, [1] Wenshuo Xu, [1] Jamie H. Warner[1]**

[1]Department of Materials, University of Oxford, Parks Road, Oxford, OX1 3PH, United Kingdom

*Jamie.warner@materials.ox.ac.uk;

Abstract

In this report, graphene (Gr) is used as a 2D electrode and monolayer WS_2 as the active semiconductor in ultrathin photodetector devices. All the 2D materials are grown by chemical vapor deposition (CVD) and thus pose as a viable route to scalability. The monolayer thickness of both electrode and semiconductor gives these photodetectors ~2 nm thickness, making them amongst the thinnest reported to date. We show that graphene is different to conventional metal (Au) electrodes due to the finite density of states from the Dirac cones of the valance and conduction bands, which enables the photoresponsivity to be modulated by electrostatic gating and light input control. We demonstrate lateral Gr-WS_2-Gr photodetectors with photoresponsivities reaching 3.5 A/W under illumination power densities of 2.5×10^7 mW/cm^2. The performance of monolayer WS_2 is compared to bilayer WS_2 in photodetectors and we show that increased photoresponsivity is achieved in the thicker bilayer WS_2 crystals due to increased optical absorption. This approach of incorporating graphene electrodes in lateral TMD based devices sheds light on the contact engineering in 2D opto-electronics, which is crucial for the development of high performing ultrathin photodetector arrays for versatile applications.

KEYWORDS: Graphene, WS_2, photodetectors, surface transfer doping, heterostructures

Two-dimensional (2D) layered materials have potential in creating the next generation of ultrathin electronics and opto-electronics devices.[1–4] In particular, 2D monolayer transition metal dichalcogenides (TMDs) such as MoS_2 and WS_2 have received considerable attention due to their semiconducting properties with a direct band gap in the visible spectrum,[5] large exciton binding energy, large absorption coefficient,[6] and sensitivity to interlayer interactions. One challenge in fabricating high-quality scalable opto-electronics with 2D TMDs is making optimized metal contacts without damage or the introduction of Fermi level pinning at the interface that causes large Schottky barrier formation. The contact resistance at the metal-semiconductor interface is often a dominating factor in TMD based electronic devices and the ability to control this interface is essential to realizing the full potential of scalable 2D TMD based electronics.[7]

To date, substantial research has been carried on metal-semiconductor-metal (MSM) structured devices to investigate the contact properties between TMD and different metal electrodes.[8–10] However, not many studies have incorporated graphene (Gr) as an electrode into these MSM devices. Prior studies have focused mainly on the electronic properties such as field-effect transistors and logic gates,[11–13] whereas the opto-electronics characteristics such as the photosensing capabilities of a Gr-TMD-Gr lateral photodetectors have yet to be fully explored. Unlike bulk metals such as Ti and Au, which are conventionally used as electrodes in TMD based electronics, graphene is highly stable and chemically inert, thus act as ideal contacts in the absence of diffusion and reaction with TMD crystals.[14] Due to graphene's finite density of states, the Fermi level of graphene can be tuned for low contact resistance[15] or even a barrier-free contact with a semiconductor.[16] For this reason, successful modulation of graphene's work function has been achieved by applying a back-gate potential,[17] electrical stressing,[18] or through defect engineering [19] and molecular doping of graphene that relies on surface charge transfer within heterostructures.[20–24] In this report we fabricate Gr-WS_2-Gr photodetectors using all CVD grown materials and examine their behavior.

Results and Discussion

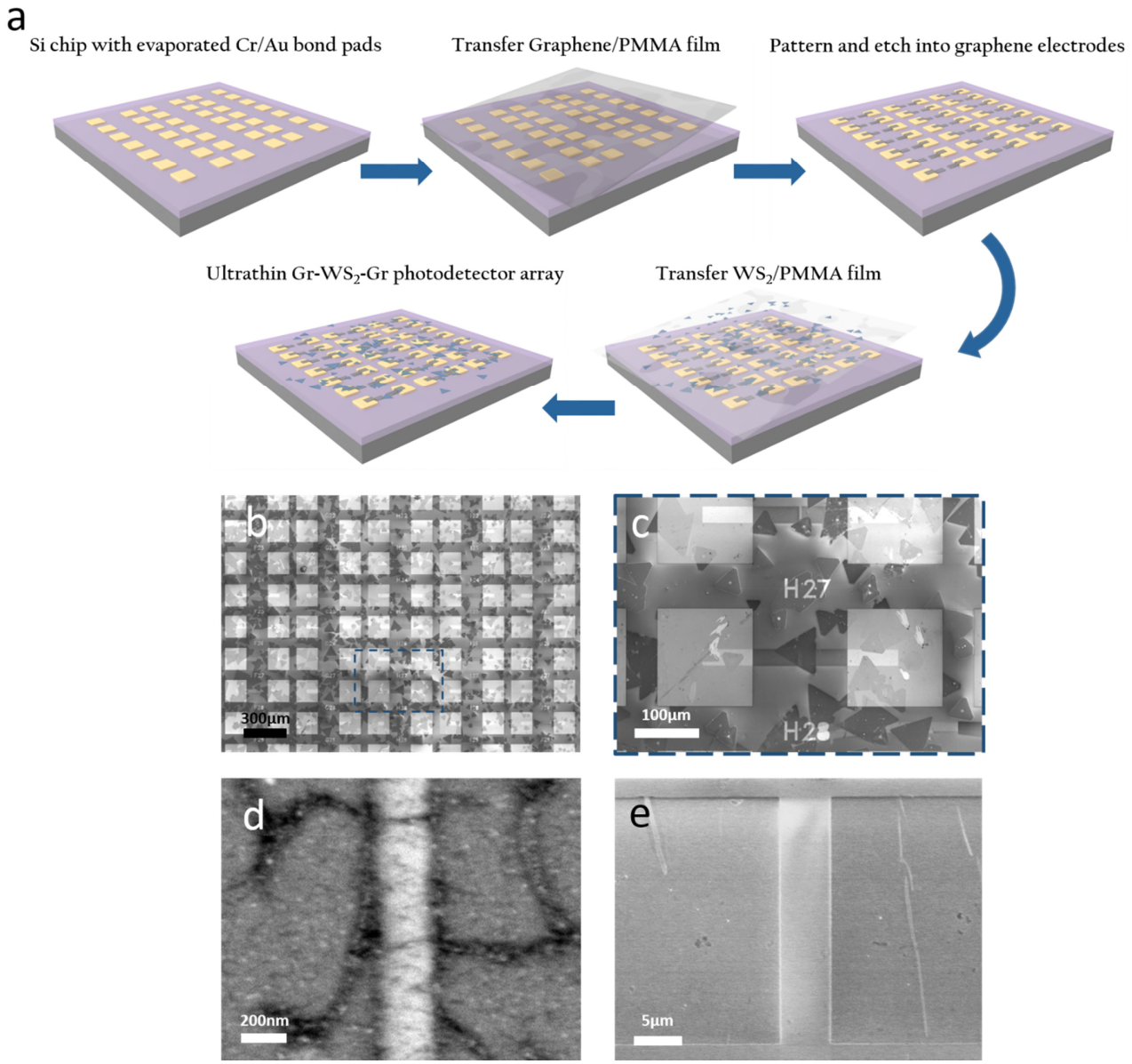

Figure 1. Fabrication and characterization of Gr-WS_2-Gr photodetector array. (a) Fabrication process schematic of Gr-WS_2-Gr photodetector array. (b) SEM image of fabricated photodetector arrays. (c) Enlarged image of framed region (blue dotted line) in (b) of a Gr-WS_2-Gr device. (d) SEM image of graphene electrode with a 200 nm wide gap. (e) SEM image of graphene electrode with a 5 μm gap. The gap between the electrodes determine the channel length of the device.

Figure 1a depicts the flow chart of the device fabrication process. Both graphene films and WS_2 domains were grown using CVD and transferred using methods reported in our previous studies.[25–27] To fabricate

the device, graphene was transferred onto a chip (Si/SiO_2 300 nm) with pre-deposited Cr/Au bond pads. The graphene was then patterned by electron-beam lithography and selectively etched by oxygen plasma into source and drain electrodes with a gap of certain width in between. A WS_2/PMMA film was subsequently transferred onto the chip consisting the metal bond pads and graphene electrodes. As shown in Figure 1b, CVD-grown WS_2 crystals are randomly distributed across the region after the transfer process, and we select the devices with WS_2 domains transferred at the center of each device, bridging the gap between the graphene electrodes, together forming a Gr-WS_2-Gr lateral photodetector. Figure 1c shows an SEM image of such a device. To better understand and characterize the performance of the photodetectors, we fabricated two different channel lengths (200 nm and 5 μm), as shown in Figure 1d-e, and explored the difference between layer number(s) (monolayer *versus* bilayer). Within the CVD grown WS_2 there are a majority of monolayer domains, but also a small number of bilayer regions, which naturally lead to a distribution of photodetector devices containing each of these types of domains. From the 500 devices on a 1 cm^2 silicon chip, about half of them have sufficient graphene coverage to make working electrodes. The subsequently transferred WS_2 step yields a ~ 20% success rate, which allows us to characterize as many as 50 Gr-WS_2-Gr devices per chip. Further work is currently underway to develop fully continuous films of TMDs that would dramatically increase device yield. However, the purpose of the study we report here is not high yield nanofabrication methods, but the fundamental study of the performance of Gr-TMD-Gr photodetectors and the total number of devices obtained with our current TMD materials is more than suitable for such investigations. Atomic Force Microscopy (AFM) topographical scan shows a typical thickness of ~2 nm for WS_2 on top of graphene. (Figure S1).

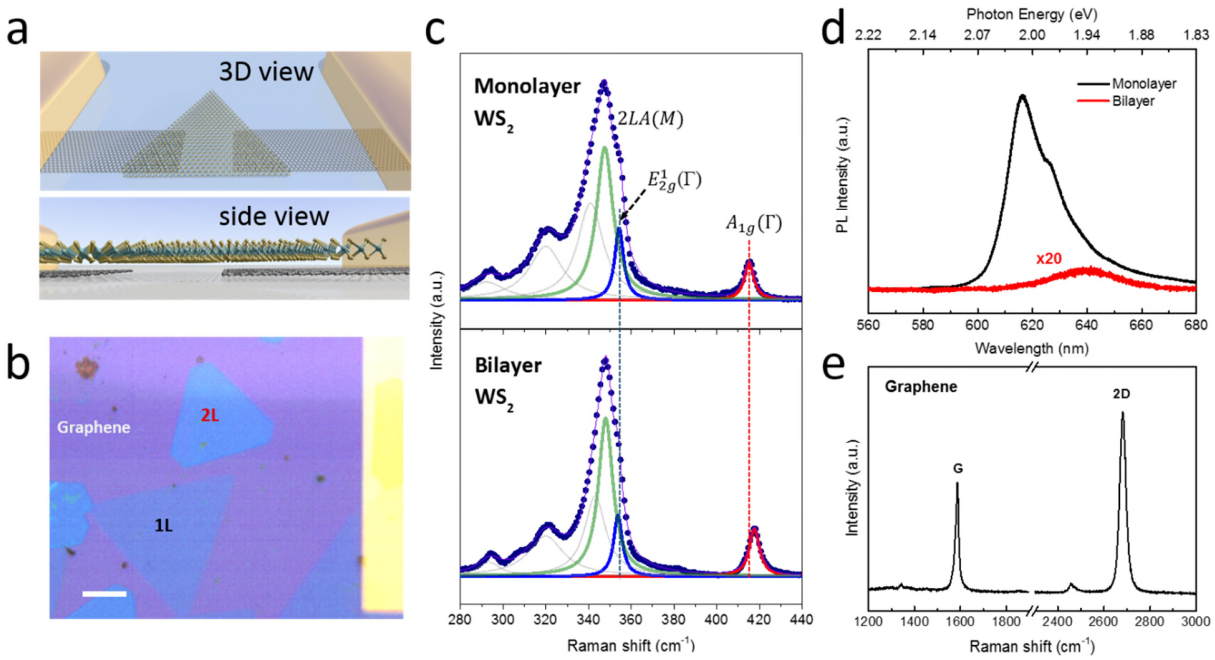

Figure 2. Raman and PL characterization of CVD-grown WS_2 and Graphene. (a) Schematic 3D and side views of Gr-WS_2-Gr photodetector (b) Optical image showing graphene, monolayer WS_2 and bilayer WS_2. Scale bar represents 20 µm (c) Raman spectra of monolayer and bilayer WS_2 under 532 nm laser. A multi-Lorentzian curve fitting of the spectra shows signature peaks of the WS_2 crystal, labeled fitted curves include the $2LA(M)$ (green), $E^1_{2g}(\Gamma)$ (blue) and $A_{1g}(\Gamma)$ (red) peaks. (d) PL spectra of monolayer and bilayer WS_2. The emission signal of bilayer WS_2 is magnified by 20 times. (e) Raman spectra of graphene electrodes. A prominent 2D peak serves as indication of monolayer graphene.

Figure 2a shows a perspective view schematic of our photodetector. Figure 2b shows an optical image that includes a graphene electrode connected to bilayer WS_2, and a monolayer domain beside the device. By optimizing the contrast of the optical image, one can easily differentiate a monolayer from a bilayer WS_2 domain. Raman spectroscopy and Photoluminescence (PL) measurements are utilized to determine the quality and layer numbers of the CVD-grown crystals. Figure 2c shows the Raman spectra of both monolayer and bilayer WS_2 under green laser with λ=532 nm. A multi-Lorentzian curve fit was performed to extract the composition peaks attributed to the different vibrational modes within the 2D systems. Here, we focus our analysis on the signals of in-plane $E^1_{2g}(\Gamma)$, out-of-plane $A_{1g}(\Gamma)$, and vibration second-order

$2LA(M)$ modes, which are commonly used to determine the thickness of WS_2 crystals.[28–30] In monolayer WS_2, the fitted peaks of $E^1_{2g}(\Gamma)$ and $A_{1g}(\Gamma)$ modes are positioned at 354.4 and 415.2 cm^{-1} respectively. As of their counterpart in bilayer, the $E^1_{2g}(\Gamma)$ mode was softened, positioning at 353.8 cm^{-1}, while the $A_{1g}(\Gamma)$ mode experienced stiffening and blue-shifts to a position of 417.7 cm^{-1}, agreeing with previous reports.[28,30] Also, the peak intensity ratio of $2LA(M)/A_{1g}(\Gamma)$ rises from 4.3 to 6.2 as layer number decrease from bilayer to monolayer, a trend consistent with previous layer-dependent Raman studies.[28] Additionally, the Raman results are further supported by the PL spectra of both crystals, showing prominent PL signal generated from the monolayer WS_2 and little emission from bilayer due to the transition of direct to indirect bandgap as layer number of WS_2 increases. The Raman spectra of graphene (Figure 1d) shows a 2D/G peak intensity ratio of around 1.5, suggesting that the CVD-grown graphene consists mostly of monolayer regions, as previously reported.[25]

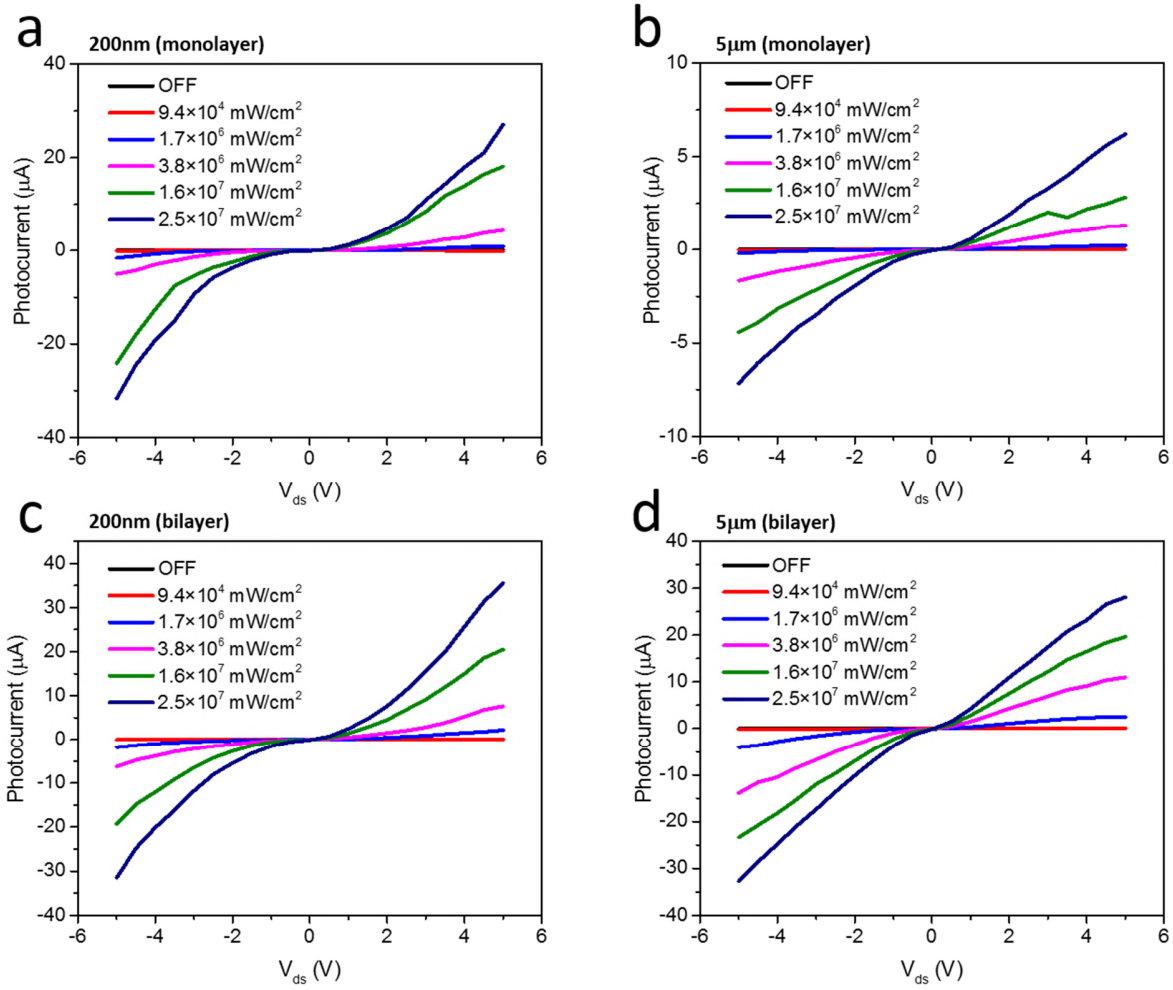

Figure 3. Bias dependent photocurrent of Gr-WS_2-Gr photodetectors. (a-d) Photocurrent of four types of devices with varying WS_2 channel length and layer numbers. 532 nm light was used for illumination.

To understand how layer number and channel length affects the photo-generated current, *I-V* measurements are carried on the devices under five different illumination intensities. Figure 3a-d show the plots of photocurrent *versus* the applied source-drain voltage on devices from all four groups. The *I-V* plots show a non-linear curve, indicative of Schottky contacts at the metal-semiconductor interface of graphene and WS_2.

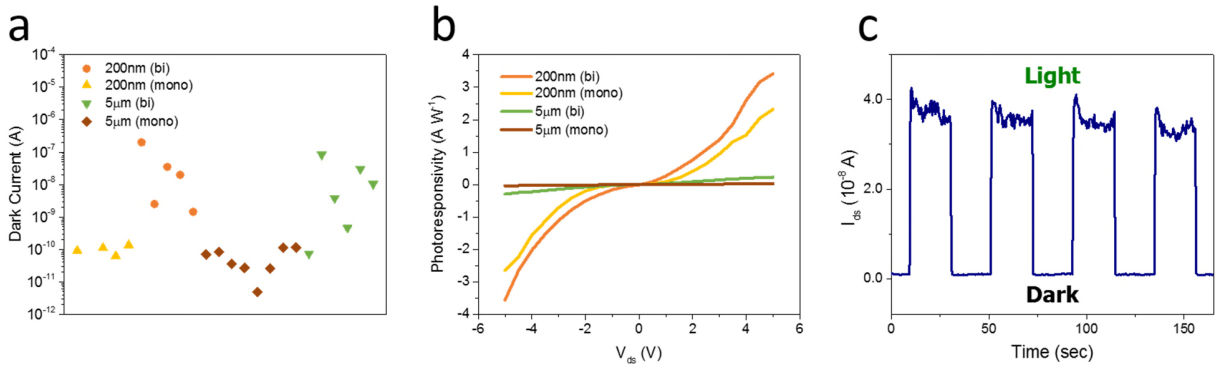

Figure 4. Photoinduced current and dark current of Gr-WS_2-Gr photodetector. (a) Dark current distribution of different types of devices under bias of +5 V. (b) Photoresponsivity of the four types of detectors under an incident light density of 3.8×10^6 mW/cm^2. (c) Transient photocurrent characteristics obtained from a device (200 nm, monolayer) under bias of +2 V with an incident light density of 3.8×10^6 mW/cm^2.

Figure 4a depicts the distribution of the dark current of twenty-three photodetectors of all four groups under an applied bias of +5 V. We find that the number of layer(s) of WS_2 has a large influence on the dark current of each devices. Though the dark current of devices in each category may fluctuate largely, overwhelming the differences caused by resistance channel length as Ohm's Law would predict, the difference between dark current in monolayer and bilayer WS_2 is clear, with the dark current of bilayer WS_2 to be around 10^{-8} A, which is two orders of magnitude larger than the monolayer's dark current of 10^{-10} A. To explain the lower resistance of bilayer WS_2 under dark conditions, we consider the following reasons. Firstly, we take into account the lower resistance brought by an extra channel for carrier transport through the second layer. The doubling of thickness more than halves the total resistance compared to the monolayer, possibly due to the low resistance edge contact formed between top layer WS_2 and graphene.[7] Secondly, we consider the passivation effect brought by the top layer of WS_2 as a capping layer. Encapsulation of the bottom WS_2 layer would isolate it from extrinsic impurities that would otherwise be introduced under direct exposure of ambient conditions,[31–33] which would lead to higher carrier mobility due to dielectric screening.[34] Photoresponsivity (R), external quantum efficiency (EQE), photogain and specific detectivity (D^*) are important figures of merit in evaluating a photodetector's performance. Photoresponsivity is a measure of a device's electrical response to incident light, defined as $R = \frac{I_{photo}}{P_{laser}}$, where

I_{photo} is the measured photocurrent, and P_{laser} is the collected illumination power. In Figure 4b we show the calculated R of the four types of devices as a function to V_{ds}, under an incident power density of 3.8×10^6 mW/cm^2. In all four types of devices, R increased with a larger applied bias, with the largest measured value under a 5 V bias to be over 3.5 A/W for a bilayer WS_2 device and 2.5 A/W for monolayer device with short channel length of 200 nm. Using the relation of

$$EQE = hcR/e\lambda \quad (1)$$

where h is the Planck constant, c is the light velocity, R is the photoresponsivity, e is the elementary charge unit, λ is the excited wavelength, we obtain EQE to be as high as 933 % and 583 % for bilayer and monolayer devices respectively. Photoresponsivity can also be expressed in terms of photogain as

$$R = \eta_{ext}Ge/h\upsilon \quad (2)$$

where η_{ext} is the external quantum efficiency, G is the photogain, and $\upsilon = \frac{c}{\lambda}$ is the frequency of incident light. Assuming that all incident photons on the photodetector are extracted in forms of charge carriers and collected as photocurrent, that is η_{ext} = 100 %, we calculate the photogain of monolayer device to be 5.8 and bilayer devices to be 9.3 (under $P_{laser} = 3.8\times10^6$ mW/cm^2, V_{bias}= +5 V). If we take into account the absorbance (~8%) and transmittance (~92%) of each layer of WS_2 under green light of each layer of WS_2,[35] we estimate the photogain of monolayer and bilayer to be 73 and 53 respectively. The higher photogain in monolayer WS_2 devices can be attributed to the high efficiency in carrier excitation under illumination due to its direct band gap. Specific detectivity (D^*) characterizes a photodetector's sensitivity by taking into account the bandwidth, geometry and noise of the device. It is given by $D^* = \frac{R\times(Af)^{1/2}}{i_n}$, where A is the effective area of the detector, f is the electrical bandwidth, and i_n is the noise current. Assuming that the dark current is dominated by shot noise, which is independent of frequency, D^* can be expressed as

$$D^* = RA^{1/2}/(2eI_{dark})^{1/2} \quad (3)$$

where I_{dark} is the measured dark current. From this we estimate the detectivity of our photodetectors to be 1.6×10^{10} Jones for bilayer devices and 9.9×10^{10} Jones for monolayer devices (Jones = cm $Hz^{1/2}$ W^{-1}).

Figure 4c shows the time-resolved photoresponse of a monolayer WS_2 device with 200 nm channel length. At a fixed bias of +2 V, reproducible low and high impedance states were obtained by switching repeated on-off cycles of light irradiation, with an on/off ratio (defined as I_{photo}/I_{dark}) of 54, allowing such a device to act as a high quality photosensitive switch. These photodetectors with graphene electrodes, showing high photoresponsivity and photogain under ambient conditions and absence of applied gate potential, are comparable and in many cases outperform reported TMD-based photodetectors with metal electrodes.[36–43] (Supporting Information S2)

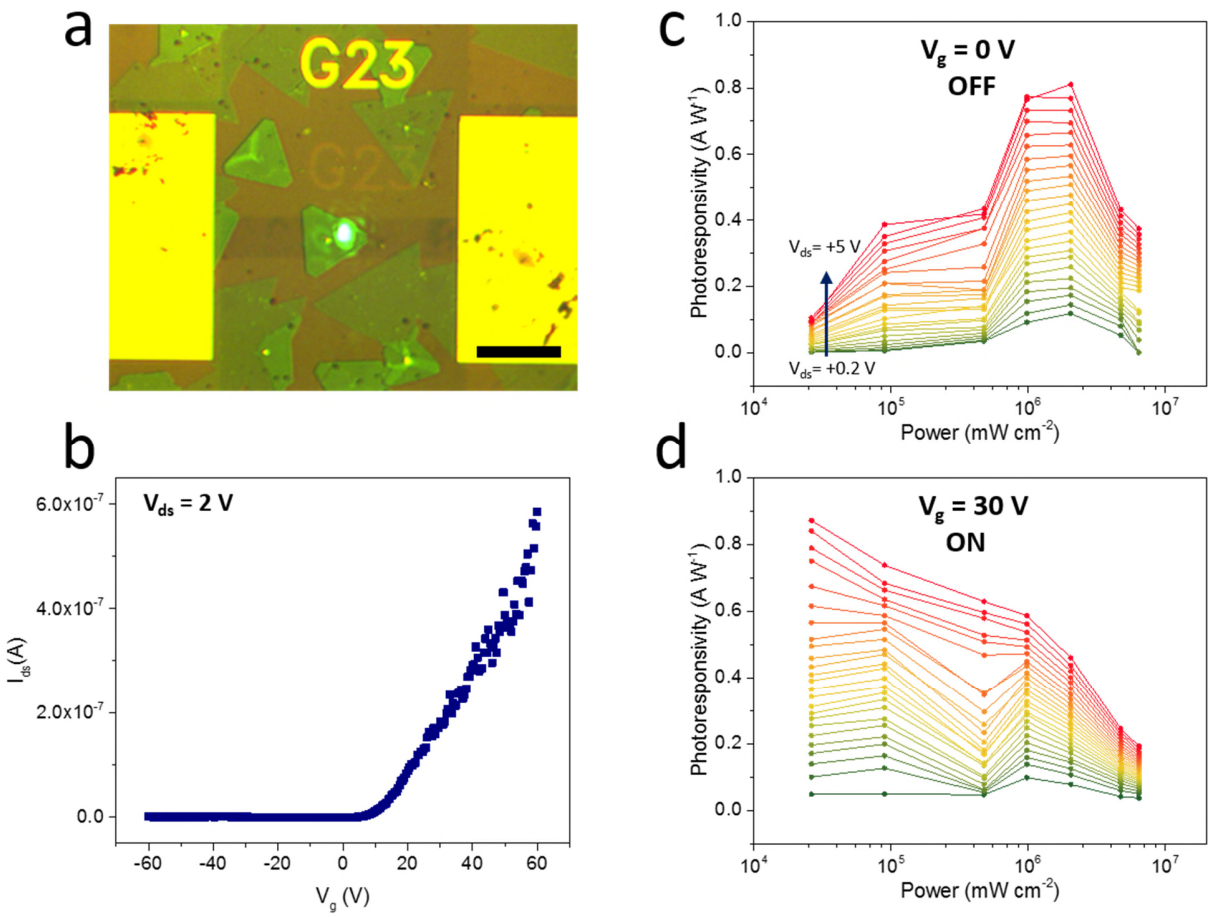

Figure 5. Photoresponsivity of WS_2 under influence of gate and illumination power. (a) Optical image of a bilayer WS_2 device illuminated by 532 nm laser. Scale bar represents 50 µm (b) Field effect of a bilayer WS_2 phototransistor. I_{ds}-V_g plot shows the N-type characteristics of the device with a threshold voltage V_{th} of ~10 V. (c-d) Photoresponsivity of bilayer WS_2 device as a function of incident light power under back gate potential of 0 V (OFF state) and 30 V (ON state) respectively.

It is worth noting that the photocurrent measurements in this study are carried under an incident light power density as high as ~10^7 mW/cm^2, which is a high value compared with many of the measurements in previous reports.[37,39,42] Under previously reported low excitation power range, a common observation in photodetector study is that photoresponsivity monotonously decreases with the increase of incident power, explained by the shortening of exciton recombination times due to the concomitant increase of generated electron-hole pairs[43] and the influence of trap states between gate oxide and the semiconductor.[44] We are thus interested in explaining the high photoresponsivity of our device under large illumination power. Figure 5a shows an illuminated bilayer WS_2 device (5 µm channel length) that was used for

gate and power dependence study. We investigate its photoresponsivity under varying applied gate potential as well as illumination power. A gate sweep measurement was carried first to show the field effect characteristics of the device. As shown in Figure 5b, the *I-V* plot shows an N-type transistor with a threshold voltage (V_{th}) of ~10 V. A power dependence study was subsequently carried with a back gate voltage of 0 V and 30 V, under which the phototransistor is tuned to its OFF and ON state respectively. Shown in Figure 5c-d, the photoresponsivity of the device show different power dependence pattern under its OFF state and ON state. Under 0 V, photoresponsivity first increases along with enhanced illumination, from 0.1 A/W under incident power density of 2×10^4 mW/cm^2 and reaches a maximum value of 0.8 A/W at a power density of 2×10^6 mW/cm^2. Above 2×10^6 mW/cm^2, photoresponsivity starts to decrease with enhanced illumination power. This power dependence trend of Gr-WS_2-Gr photodetector's photoresponsivity is very different compared with the behavior of an Au-WS_2-Au photodetector, which decreased monotonously with increasing incident power (Supporting Information S3). Under 30 V, when the Gr-WS_2-Gr transistor is switch into its ON state, the photoresponsivity then starts to follow a negative correlation with illumination power, exhibiting the highest photoresponse under the lowest applied laser power density of 2×10^4 mW/cm^2. Based on our recent findings on light-induced charge transfer between graphene and WS_2,[23] we propose that such an increase in photoresponsivity with enhanced incident light can be attributed to the unique contact between graphene and WS_2.

Figure 6a-c show a schematic of band structure at the graphene and WS_2 interface at a non-equilibrium condition. It has been well documented that the resistivity of a metal-semiconductor contact is greatly influenced by the Schottky barrier formed at its heterojunctions.[45] Under assumption of the Schottky-Mott rule, the height of the Schottky barrier, denoted as Φ_{SB}, is determined by the band offset at the Gr/WS_2 interface, which can be expressed as $\Phi_{\mathrm{SB}} = \Phi_{Gr} - \chi_{WS_2}$, where Φ_{Gr} is the work function of graphene (~4.6 eV)[17] and χ_{WS_2} the electron affinity of WS_2 (~4.0 eV).[46] Thus we estimate a Schottky barrier height of $\Phi_{\mathrm{SB}} = 0.6$ eV between graphene and WS_2. As positive gate potential is applied, electrons are induced in graphene which caused a decrease in graphene's work function, resulting in a lower-

ing of barrier height (Figure 6b). To further study this relationship between barrier height and gate potential, we introduce a back-to-back Schottky diode model as a simple representation of our MSM photodetector, and have fitted the *I-V* measurements of devices under increasing applied back-gate using a modified thermionic emission equation (Supporting Information S4). It is found that the obtained Φ_{SB} monotonously decreased with increasing positive gate potential, and at Vg = +70 V, reached a lowest value to 0.33 eV and 0.26 eV for monolayer and bilayer devices respectively (Figure 6d and 6e). This modification of the Schottky barrier for Gr-TMD contacts due to the tunable work function of graphene has been observed in several prior reports and is therefore expected here as well.[15,24,47,48] However, similar gate dependence of Schottky barrier height were not observed in our WS_2 devices with Au electrodes (Supporting Information S3), which could be due to Fermi level pinning attributing to the existence of trap states at the Au-WS_2 interface, discussed in our previous work.[49] To explain the light modulated photoresponsivity, we turn to the photoinduced charge transfer in graphene/WS_2 heterostructure which has been observed in a previous study.[23] This surface charge transfer process generates layer-separated electron-hole pairs, with electrons residing in graphene and holes located in WS_2, resulting in the n-doping of graphene (Figure 6c). This would increase the Fermi level of graphene and lower the contact resistance of the photodetector. We propose that this photo-gating mechanism could serve as an explanation for our devices' improved photoresponsivity under high illumination power. Once the Gr-WS_2-Gr phototransistor is switched into the ON state under an applied gate potential larger than V_{th}, the influence of illumination on the Fermi level is reduced and thus results in a different power dependence of photoresponsivity shown in Figure 5c-d.

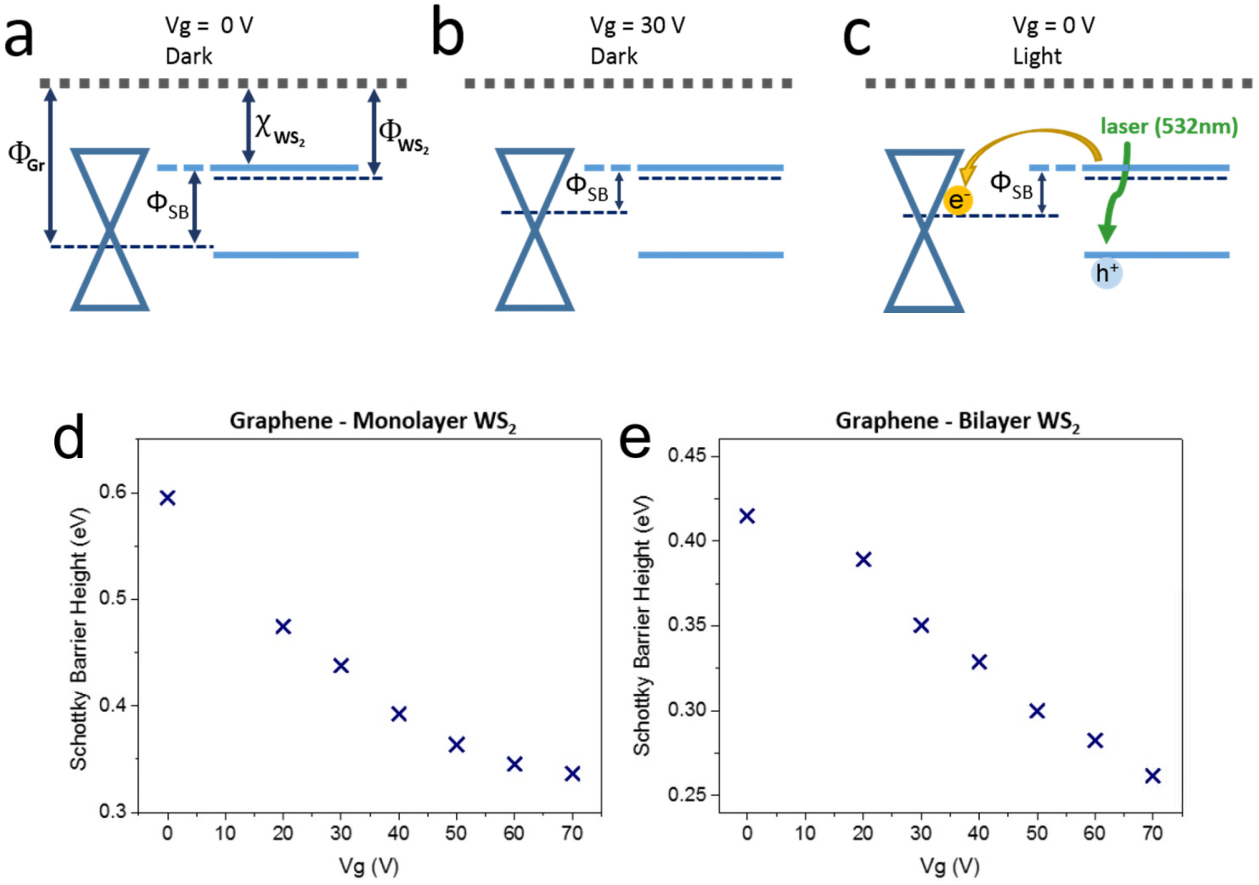

Figure 6. Mechanism for photoresponsivity increase with added positive gate and illumination power. (a,b,c) Schematic of band diagram of Gr/WS_2 heterostructure under non-equilibrium condition, depicting the work function of graphene Φ_{Gr} and electron affinity of WS_2 χ_{WS_2} relative to vacuum level under different back gate potential and illumination conditions. Both positive applied gate potential and illumination of the heterostructured regions cause Fermi level of graphene to rise, which results in the lowering of graphene-WS_2 Schottky barrier Φ_{SB}. Schottky barrier height as a function of back gate potential Vg for (d) Graphene-monolayer WS_2, and (e) Graphene-bilayer WS_2. The effective height of Schottky barrier monotonically decreases with increasing positive gate potential.

Conclusion

In summary, we have demonstrated the fabrication of ultrathin lateral MSM WS_2 photodetectors using graphene as electrodes. We believe that this is the first case where all 2D based lateral photodetectors have been produced using materials only grown by CVD, eliminating mechanical exfoliation from the process. The Gr-WS_2-Gr photodetectors exhibit high photoresponse reaching ~3.5 A/W under ambient atmosphere and high input visible light at 532 nm. The outstanding performance of the device can be attributed to the modulation of the Schottky barrier between graphene and WS_2 under an applied gate and increased illumination power. We conclude that graphene electrodes serve as an ideal medium for carrier transport for MSM photodetectors, with a gate and light tunable contact resistance with WS_2 due to its limited density of states, and enhanced photoresponsivity under increasing illumination power due to efficient light-induced charge transfer between WS_2. This interesting behavior could lead to new designs of photodetectors which could maintain a high photoresponse under strong light power detection.

Experimental Methods

CVD growth of monolayer Graphene and WS_2

Monolayer graphene was grown using our previously reported method involving deposition on liquid Cu with tungsten substrate.[25] Graphene was grown on the melted Cu with a flow of 200 sccm Argon, 30 sccm Hydrogen (25%) and 10 sccm of Methane (1%) for 90 min, subsequently followed by a secondary growth process at 1060^{o}C for 30 min. The sample was then removed from the heating zone and cooled to room temperature. WS_2 crystals were grown on 90 nm SiO_2/Si substrate using our previously reported method.[27] The two precursors, sulphur powder (400 mg of purum grade 99.5%) and WO_3 (200 mg of puriss grade 99.9%) are placed separately in a double-walled-quartz-tube. Sulphur and WO_3 powder were positioned in the external and internal tube respectively and heated by two furnace systems. Vaporized precursors are brought to the reaction zone by argon gas flow, where WO_3 undergoes sulfurization. The as-grown WS_2 samples were fast cooled as soon as the reaction is completed.

Transfer of CVD grown graphene and WS_2

The as-grown CVD samples were first spin-coated with a poly(methyl methacrylate) (PMMA) scaffold (8 wt% in anisole, 495k molecular weight). Tungsten substrate of the Graphene sample was electrochemically etched in NaOH (2 M) by connecting a 2.4 V on the sample and using a Cu foil as anode.[26] The PMMA/Graphene film was then separated from Cu substrate by $(NH_4)_2S_2O_8$ etching (0.1 M). The PMMA/WS_2 film was separated from the SiO_2/Si substrate by KOH etching (1 M) at 60°C. The floating PMMA/Graphene and PMMA/WS_2 films were carefully transferred several times into deionized water for cleansing purposes. The films were subsequently transferred onto Si chip and baked at 150 °C for 30 min for sample adhesion.

Device fabrication

JEOL 5500 FS EBL system was used to pattern bond pads in a bilayer PMMA resist. A thermal evaporator was used to deposit Cr/Au (10 nm/80 nm) bond pads onto a 300 nm SiO_2/Si substrate, followed by liftoff in hot acetone. Graphene/PMMA film was transferred onto the Si chip with pre-patterned bond pads, and baked overnight at 180°C for better contact. Graphene film was then patterned using EBL with negative resist and oxygen plasma etching to define graphene channels with a length and width of 100 μm and 25 μm respectively. Gaps of differing length (200 nm and 5 μm) between graphene channels were fabricated using the same process. Lastly, WS_2/PMMA film was transferred onto the sample.

Opto-electronic characterization of devices

Raman and PL spectroscopy was carried out using a LabRam Aramis Raman Spectrometer. Samples are illuminated with a 532 nm laser of 200 μW, through a ×50 objective lens with a spot size of ~2 μm. A Keithley 2400 source meter was used for *I-V* characteristics and responsivity of the Gr-WS_2-Gr photodetectors. For illumination during photoresponse measurements, a 532 nm diode-pumped solid-state laser (Thorlabs, DJ532-40) which was coupled into a confocal microscope to form a beam with spot size of ~150 μm^2 as a light source. The power values of the output laser are taken by a manually fixated power

meter (Thorslab Optics PM100D, ±3 % accuracy) placed above the devices before each *I-V* measurement. Tungsten tips connected to a Keithley 2400 source meter are used to probe the metal bond-pads of each devices and to apply a bias sweep from -5 V to +5 V.

Supporting Information

The Supporting Information is available free of charge on the ACS Publications website at DOI:

AFM measurements of Gr-WS_2 stack. Table of comparative results for TMD based photodetector's photoresponsivity. Comparative study with Au-WS_2-Au photodetector. Details of gate dependence study of Gr-WS_2 Schottky barrier height determination.

Acknowledgements

J.H.W thanks the support from the Royal Society and Samsung. H. T. thanks Yayasan Khazanah for funding the Merdeka Scholarship.

References

(1) Wang, Q. H.; Kalantar-Zadeh, K.; Kis, A.; Coleman, J. N.; Strano, M. S. Electronics and Optoelectronics of Two-Dimensional Transition Metal Dichalcogenides. *Nat. Nanotechnol.* **2012**, *7*, 699–712.

(2) Koppens, F. H. L.; Mueller, T.; Avouris, P.; Ferrari, A. C.; Vitiello, M. S.; Polini, M. Photodetectors Based on Graphene, Other Two-Dimensional Materials and Hybrid Systems. *Nat. Nanotechnol.* **2014**, *9*, 780–793.

(3) Jariwala, D.; Sangwan, V. K.; Lauhon, L. J.; Marks, T. J.; Hersam, M. C. Emerging Device Applications for Semiconducting Two-Dimensional Transition Metal Dichalcogenides. *ACS Nano* **2014**, *8*, 1102–1120.

(4) Buscema, M.; Island, J. O.; Groenendijk, D. J.; Blanter, S. I.; Steele, G. A.; Van der Zant, H. S.; Castellanos-Gomez, A. Photocurrent Generation with Two-Dimensional van Der Waals Semiconductors. *Chem Soc Rev* **2015**, *44*, 3691–3718.

(5) Mak, K. F.; Lee, C.; Hone, J.; Shan, J.; Heinz, T. F. Atomically Thin MoS2: A New Direct-Gap Semiconductor. *Phys. Rev. Lett.* **2010**, *105*, 136805.

(6) Ganatra, R.; Zhang, Q. Few Layer MoS2 - A Promising Layered Semiconductor. *ACS Nano* **2014**, 8, 4047-4099.

(7) Allain, A.; Kang, J.; Banerjee, K.; Kis, A. Electrical Contacts to Two-Dimensional Semiconductors. *Nat. Mater.* **2015**, *14*, 1195–1205.

(8) Zhang, W.; Chiu, M.-H.; Chen, C.-H.; Chen, W.; Li, L.-J.; Wee, A. T. S. Role of Metal Contacts in High-Performance Phototransistors Based on WSe2 Monolayers. *ACS Nano* **2014**, *8*, 8653–8661.

(9) Das, S.; Chen, H.-Y.; Penumatcha, A. V.; Appenzeller, J. High Performance Multilayer MoS2

Transistors with Scandium Contacts. *Nano Lett.* **2013**, *13*, 100–105.

(10) Wang, W.; Liu, Y.; Tang, L.; Jin, Y.; Zhao, T.; Xiu, F. Controllable Schottky Barriers between MoS2 and Permalloy. *Sci. Rep.* **2014**, *4*, 6928.

(11) Yu, L.; Lee, Y. H.; Ling, X.; Santos, E. J. G.; Shin, Y. C.; Lin, Y.; Dubey, M.; Kaxiras, E.; Kong, J.; Wang, H.; Palacios, T. Graphene/MoS2 Hybrid Technology for Large-Scale Two-Dimensional Electronics. *Nano Lett.* **2014**, *14*, 3055–3063.

(12) Roy, T.; Tosun, M.; Kang, J. S.; Sachid, A. B.; Desai, S. B.; Hettick, M.; Hu, C. C.; Javey, A. Field-Effect Transistors Built from All Two-Dimensional Material Components. *ACS Nano* **2014**, *8*, 6259–6264.

(13) Chuang, H.-J.; Tan, X.; Ghimire, N. J.; Perera, M. M.; Chamlagain, B.; Cheng, M. M.-C.; Yan, J.; Mandrus, D.; Tománek, D.; Zhou, Z. High Mobility WSe2 P- and N-Type Field-Effect Transistors Contacted by Highly Doped Graphene for Low-Resistance Contacts. *Nano Lett.* **2014**, *14*, 3594–3601.

(14) Mcdonnell, S.; Addou, R.; Buie, C.; Wallace, R. M.; Hinkle, C. L. Defect-Dominated Doping and Contact Resistance in MoS 2. *ACS Nano* **2014**, *8*, 2880–2888.

(15) Shih, C. J.; Wang, Q. H.; Son, Y.; Jin, Z.; Blankschtein, D.; Strano, M. S. Tuning on-off Current Ratio and Field-Effect Mobility in a MoS2-Graphene Heterostructure *via* Schottky Barrier Modulation. *ACS Nano* **2014**, *8*, 5790–5798.

(16) Liu, Y.; Wu, H.; Cheng, H. C.; Yang, S.; Zhu, E.; He, Q.; Ding, M.; Li, D.; Guo, J.; Weiss, N. O.; Huang, Y.; Duan, X. Toward Barrier Free Contact to Molybdenum Disulfide Using Graphene Electrodes. *Nano Lett.* **2015**, *15*, 3030–3034.

(17) Yu, Y.-J.; Zhao, Y.; Ryu, S.; Brus, L. E.; Kim, K. S.; Kim, P. Tuning the Graphene Work Function by Electric Field Effect. *Nano Lett.* **2009**, *9*, 3430–3434.

(18) Chiu, H.-Y.; Perebeinos, V.; Lin, Y.-M.; Avouris, P. Controllable P-N Junction Formation in Monolayer Graphene Using Electrostatic Substrate Engineering. *Nano Lett.* **2010**, *10*, 4634–4639.

(19) Usachov, D.; Vilkov, O.; Grüneis, A.; Haberer, D.; Fedorov, A.; Adamchuk, V. K.; Preobrajenski, A. B.; Dudin, P.; Barinov, A.; Oehzelt, M.; Laubschat, C.; Vyalikh, D. V. Nitrogen-Doped Graphene: Efficient Growth, Structure, and Electronic Properties. *Nano Lett.* **2011**, *11*, 5401–5407.

(20) Chen, W.; Chen, S.; Qi, D. C.; Gao, X. Y.; Wee, A. T. S. Surface Transfer P-Type Doping of Epitaxial Graphene. *J. Am. Chem. Soc.* **2007**, *129*, 10418–10422.

(21) Konstantatos, G.; Badioli, M.; Gaudreau, L.; Osmond, J.; Bernechea, M.; De Arquer, F. P. G.; Gatti, F.; Koppens, F. H. L. Hybrid Graphene-Quantum Dot Phototransistors with Ultrahigh Gain. *Nat Nano* **2012**, *7*, 363–368.

(22) Ju, L.; Velasco, J.; Huang, E.; Kahn, S.; Nosiglia, C.; Tsai, H.-Z.; Yang, W.; Taniguchi, T.; Watanabe, K.; Zhang, Y.; Zhang, G.; Crommie, M.; Zettl, A.; Wang, F. Photoinduced Doping in Heterostructures of Graphene and Boron Nitride. *Nat. Nanotechnol.* **2014**, *9*, 348–352.

(23) Tan, H.; Fan, Y.; Rong, Y.; Porter, B.; Lau, C. S.; Zhou, Y.; He, Z.; Wang, S.; Bhaskaran, H.; Warner, J. H. Doping Graphene Transistors Using Vertical Stacked Monolayer WS2 Heterostructures Grown by Chemical Vapor Deposition. *ACS Appl. Mater. Interfaces* **2016**, 8, 1644-1652.

(24) Rathi, S.; Lee, I.; Lim, D.; Wang, J.; Ochiai, Y.; Aoki, N.; Watanabe, K.; Taniguchi, T.; Lee, G.-H.; Yu, Y.-J.; Kim, P.; Kim, G.-H. Tunable Electrical and Optical Characteristics in Monolayer Graphene and Few-Layer MoS2 Heterostructure Devices. *Nano Lett.* **2015**, *15*, 5017–5024.

(25) Wu, Y. A.; Fan, Y.; Speller, S.; Creeth, G. L.; Sadowski, J. T.; He, K.; Robertson, A. W.; Allen, C. S.; Warner, J. H. Large Single Crystals of Graphene on Melted Copper Using Chemical Vapor Deposition. *ACS Nano* **2012**, *6*, 5010–5017.

(26) Fan, Y.; He, K.; Tan, H.; Speller, S.; Warner, J. H. Crack-Free Growth and Transfer of Continuous Monolayer Graphene Grown on Melted Copper. *Chem. Mater.* **2014**, *26*, 4984–4991.

(27) Rong, Y.; Fan, Y.; Leen Koh, A.; Robertson, A. W.; He, K.; Wang, S.; Tan, H.; Sinclair, R.; Warner, J. H. Controlling Sulphur Precursor Addition for Large Single Crystal Domains of WS2. *Nanoscale* **2014**, *6*, 12096–12103.

(28) Berkdemir, A.; Gutiérrez, H. R.; Botello-Méndez, A. R.; Perea-López, N.; Elías, A. L.; Chia, C.-I.; Wang, B.; Crespi, V. H.; López-Urías, F.; Charlier, J.-C.; Terrones, H.; Terrones, M. Identification of Individual and Few Layers of WS2 Using Raman Spectroscopy. *Sci. Rep.* **2013**, *3*, 1755.

(29) Zeng, H.; Liu, G.-B.; Dai, J.; Yan, Y.; Zhu, B.; He, R.; Xie, L.; Xu, S.; Chen, X.; Yao, W.; Cui, X. Optical Signature of Symmetry Variations and Spin-Valley Coupling in Atomically Thin Tungsten Dichalcogenides. *Sci. Rep.* **2013**, *3*, 1608.

(30) He, Z.; Rong, Y.; Smith, J.; Warner, J. H. Biexciton Formation in Bilayer Tungsten Disulfide. *ACS Nano* **2016**, 10, 2176-2183.

(31) Late, D. J.; Liu, B.; Matte, H. S. S. R.; Dravid, V. P.; Rao, C. N. R. Hysteresis in Single-Layer MoS2 Field Effect Transistors. *ACS Nano* **2012**, *6*, 5635–5641.

(32) Withers, F.; Bointon, T. H.; Hudson, D. C.; Craciun, M. F.; Russo, S. Electron Transport of WS2 Transistors in a Hexagonal Boron Nitride Dielectric Environment. *Sci. Rep.* **2014**, *4*, 4967.

(33) Ovchinnikov, D.; Allain, A.; Huang, Y. S.; Dumcenco, D.; Kis, A. Electrical Transport Properties of Single-Layer WS2. *ACS Nano* **2014**, *8*, 8174–8181.

(34) Kufer, D.; Konstantatos, G. Highly Sensitive, Encapsulated MoS2 Photodetector with Gate Controllable Gain and Speed. *Nano Lett.* **2015**, *15*, 7307–7313.

(35) Bernardi, M.; Palummo, M.; Grossman, J. C. Extraordinary Sunlight Absorption and One Nanometer Thick Photovoltaics Using Two-Dimensional Monolayer Materials. *Nano Lett.* **2013**, *13*, 3664–3670.

(36) Perea-López, N.; Elías, A. L.; Berkdemir, A.; Castro-Beltran, A.; Gutiérrez, H. R.; Feng, S.; Lv, R.; Hayashi, T.; López-Urías, F.; Ghosh, S.; Muchharla, B.; Talapatra, S.; Terrones, H.; Terrones, M. Photosensor Device Based on Few-Layered WS2 Films. *Adv. Funct. Mater.* **2013**, *23*, 5511–5517.

(37) Huo, N.; Yang, S.; Wei, Z.; Li, S.-S.; Xia, J.-B.; Li, J. Photoresponsive and Gas Sensing Field-Effect Transistors Based on Multilayer WS_2 Nanoflakes. *Sci. Rep.* **2014**, *4*, 5209.

(38) Yin, Z.; Li, H.; Li, H.; Jiang, L.; Shi, Y.; Sun, Y.; Lu, G.; Zhang, Q.; Chen, X.; Zhang, H. Single-Layer MoS2 Phototransistors. *ACS Nano* **2012**, *6*, 74–80.

(39) Zhang, W.; Huang, J. K.; Chen, C. H.; Chang, Y. H.; Cheng, Y. J.; Li, L. J. High-Gain Phototransistors Based on a CVD MoS2 Monolayer. *Adv. Mater.* **2013**, *25*, 3456–3461.

(40) Tsai, D.-S.; Liu, K.-K.; Lien, D.-H.; Tsai, M.-L.; Kang, C.-F.; Lin, C.-A.; Li, L.-J.; He, J.-H. Few Layer MoS2 with Broadband High Photogain and Fast Optical Switching for Use in Harsh Environments. *ACS Nano* **2013**, 3905–3911.

(41) Xia, J.; Huang, X.; Liu, L. Z.; Wang, M.; Wang, L.; Huang, B.; Zhu, D. D.; Li, J. J.; Gu, C. Z.; Meng, X. M. CVD Synthesis of Large-Area, Highly Crystalline MoSe2 Atomic Layers on Diverse Substrates and Application to Photodetectors. *Nanoscale* **2014**, *6*, 8949–8955.

(42) Abderrahmane, A.; Ko, P. J.; Thu, T. V; Ishizawa, S.; Takamura, T.; Sandhu, A. High

Photosensitivity Few-Layered MoSe2 Back-Gated Field-Effect Phototransistors. *Nanotechnology* **2014**, *25*, 365202.

(43) Pradhan, N.; Ludwig, J.; Lu, Z.; Rhodes, D.; Bishop, M. M.; Thirunavukkuarasu, K.; McGill, S.; Smirnov, D.; Balicas, L. High Photoresponsivity and Short Photo Response Times in Few-Layered WSe_2 Transistors. *ACS Appl. Mater. Interfaces* **2015**, 7, 12080-12088.

(44) Lopez-Sanchez, O.; Lembke, D.; Kayci, M.; Radenovic, A.; Kis, A. Ultrasensitive Photodetectors Based on Monolayer MoS2. *Nat. Nanotechnol.* **2013**, *8*, 497–501.

(45) Sze, S. M.; Ng, K. K. *Physics of Semiconductor Devices*, John Wiley & Sons: New York, 2006.

(46) Yamaguchi, T.; Moriya, R.; Inoue, Y.; Morikawa, S.; Masubuchi, S.; Watanabe, K.; Taniguchi, T.; Machida, T. Tunneling Transport in a Few Monolayer-Thick WS2/Graphene Heterojunction. *Appl. Phys. Lett.* **2014**, *105*, 223109.

(47) Yu, W. J.; Liu, Y.; Zhou, H.; Yin, A.; Li, Z.; Huang, Y.; Duan, X. Highly Efficient Gate-Tunable Photocurrent Generation in Vertical Heterostructures of Layered Materials. *Nat. Nanotechnol.* **2013**, *8*, 952–958.

(48) Tian, H.; Tan, Z.; Wu, C.; Wang, X.; Mohammad, M. A.; Xie, D.; Yang, Y.; Wang, J.; Li, L.-J.; Xu, J.; Ren, T.-L. Novel Field-Effect Schottky Barrier Transistors Based on Graphene-MoS2 Heterojunctions. *Sci. Rep.* **2014**, *4*, 5951.

(49) Fan, Y.; Zhou, Y.; Wang, X.; Tan, H.; Rong, Y.; Warner, J. H. Photoinduced Schottky Barrier Lowering in 2D Monolayer WS2 Photodetectors. *Adv. Opt. Mater.* **2016**, *Early View*, DOI: 10.1002/adom.201600221

TOC graphic